Journal of Sound and Vibration (1994) **178**(1), 67–77

WIND-INDUCED DYNAMICS OF A DEEP SPACE NETWORK ANTENNA

W. GAWRONSKI

Jet Propulsion Laboratory, California Institute of Technology, Pasadena, California 91109, *U.S.A.*

B. BIENKIEWICZ

Civil Engineering Department, Colorado State University, Fort Collins, Colorado 80523, *U.S.A.*

AND

R. E. HILL

Hill Engineering Services, Glendale, California 91214, *U.S.A.*

(*Received* 5 *October* 1992, *and in final form* 22 *July* 1993)

Accurate spacecraft tracking by the NASA Deep Space Network (DSN) antennas must be assured during changing weather conditions. Wind disturbances are the main source of antenna vibrations, and consequently tracking errors. A wind force model is developed, and simulation results of wind-induced vibrations and pointing errors of the DSN antennas are presented. The antenna model includes the antenna structure, the elevation and azimuth servos, and the tracking controller. Simulation results show that pointing errors due to wind gusts are of the same order as errors due to wind steady state pressure, and that (similarly to steady state wind pressure) these errors satisfy the velocity quadratic law. The methodology presented is next used for wind disturbance estimation and for design of an antenna controller with wind disturbance rejection properties.

1. INTRODUCTION

Reliable estimates of tracking errors due to wind disturbances are required for NASA Deep Space Network (DSN) antenna operational purposes, as well as for the design of effective controllers. There are three types of wind-induced pointing errors; steady state errors due to steady state wind pressure, dynamic errors due to wind turbulence, and the errors due to flow separation. Steady state error models of antennas have been investigated by Katow and McGinness [1] and Katow [2], and dynamic errors of the DSS-14 antenna have been analyzed by Massoudi [3]. The errors due to flow separation have not yet been analyzed for the antennas.

The purpose of this paper is to illustrate the use of the available wind models and test data to obtain reliable tools for vibration simulation of a large flexible structure. This goal is achieved by simulating gust forces based on the Davenport spectrum of wind velocity. Since no linear system exists to produce time series with the Davenport spectrum, a linear filter has been developed which generates a wind force with a spectrum optimally close to the Davenport spectrum. This allows use of the steady state wind tunnel data to generate steady state as well as gust forces.

The analysis of antenna response and tracking involves a complex computational procedure. To make the problem reasonable, a simple but non-trivial approach has been

0022-460X/94/460067 + 11 $08.00/0

chosen. A perfect coherence of a flow is assumed, and the flow separation and wake effects are neglected. The perfect coherence assumption is expected to result in the overestimation of wind force, increasing with frequency. The discarding of the flow separation and wake effects leads to an underestimation of the wind force and an inability to account for possible aeroelastic effects. The qualitative effects of the above assumptions and simplifications are not available yet and will need separate studies, based on wind tunnel tests. The choice of the Davenport spectrum for the wind gusts model has been made based on its simplicity. However, the updated Kaimal model has been also used for comparison, showing good coincidence.

In this paper, the DSS-13 antenna (Figure 1), representative of the recent generation of 34 m (dish diameter) antennas, is analyzed. A recently developed antenna model by Gawronski and Mellstrom [4] has been used to analyze wind disturbances. The structural finite element model, as a part of the antenna model, includes modes of up to 10 Hz. The dynamic wind pressure consists of the spatial pressure on the antenna structure and the wind force time history. In the new approach presented in this paper, the wind force [10], is modelled as a pressure on the antenna dish rather than as an equivalent elevation torque, which is commonly used in the antenna and radar industry as a replacement for wind action [5]. The wind pressure distribution is obtained from the JPL/IDEAS finite element code (Levy and Strain [6]), based on wind tunnel measurements (Fox [7], Blaylock [8] and Levy and Kurtz [9]). The wind force time history is another new addition. It is obtained

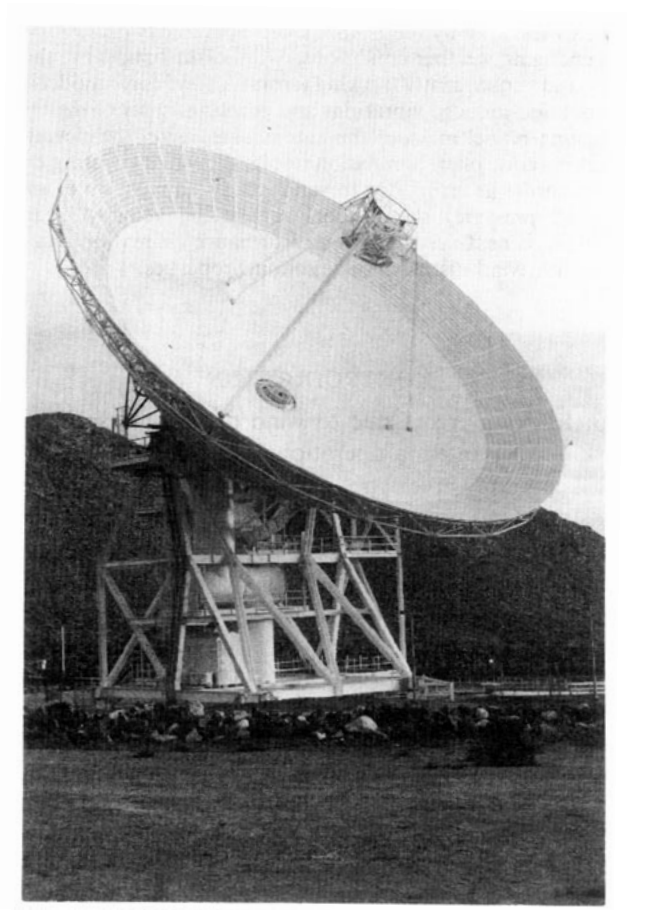

Figure 1. The DSS-13 antenna at Goldstone, California.

from the Davenport wind velocity spectrum, and an optimal linear filter shapes the wind force time profile.

The antenna vibrations can be described by many variables (such as dish or tripod vibrations, torques and rates of control system), but the ultimate characteristics of a tracking antenna are its pointing errors in azimuth and elevation. Therefore, in this paper are presented the results of pointing error simulations as a summary of the performance of tracking in a windy environment. The results are obtained, for steady state wind pressure and for wind gusts, for the antenna tracking near elevation angles of 60 and 90 degrees.

2. WIND VELOCITY AND WIND FORCE MODELS

Wind velocity v is a combination of steady state flow v_m (mean velocity, or quasi-steady component, see Levy and McGinnes [11]), and a turbulence (gust) v_t:

$$v = v_m + v_t. \tag{1}$$

The component v_t is a random process with zero mean, and standard deviation σ_v. The standard deviation as well as other gust parameters are determined from the Davenport model [10]. In this model, the wind velocity spectrum S_v for the wind at height 10 m is as follows:

$$S_v(f) = 4v_s^2 f^{-1} x^2/(1 + x^2)^{4/3}, \tag{2}$$

where f is the frequency (Hz), v_s is the shear velocity of the flow (m/s), x is the dimensionless frequency $x = 1200f/v_m$ and v_m (m/s) is the mean velocity at 10 m. Denoting $\kappa = (v_s/v_m)^2$ as the surface drag coefficient, equation (2) gives

$$S_v(f) = 4800 v_m \kappa x/(1 + x^2)^{4/3}. \tag{3}$$

The surface drag coefficient is obtained from the roughness of the terrain, cf., Simiu and Scanlan [12], as

$$\kappa = (2{\cdot}5 \ln (z/z_0))^{-2} \tag{4}$$

where z is the distance from the ground ($z = 10$ m), and z_0 is the roughness length (5–20 cm in the DSS-13 environment). For the roughness $z_0 = 0{\cdot}05$ m, one obtains $\kappa = 0{\cdot}0057$, and for $\kappa_0 = 0{\cdot}2$ m, $\kappa = 0{\cdot}0105$, which are in agreement with the Levy and McGinness [11] estimates of κ at the DSS-13 antenna site in Goldstone, California.

It is well known (see Bendat and Piersol [13]) that the standard deviation of a stationary process is determined from its spectrum, namely

$$\sigma_v = \sqrt{T_v(\omega) - T_v(0)}, \tag{5a}$$

where

$$T_v(f) = \int_0^f S_v(v)\, dv = 6\kappa v_m^2 (1 - (1 + x)^{-1/3}); \tag{5b}$$

thus

$$\sigma_v = \alpha v_m, \qquad \alpha = \sqrt{6\kappa}. \tag{6}$$

For a typical surface drag coefficient of $\kappa = 0{\cdot}005$–$0{\cdot}010$ one obtains $\alpha = 0{\cdot}17$–$0{\cdot}25$.

Although the force is acting on the whole antenna structure, in this approach (due to availability of the experimental data) the wind force is assumed to act on the antenna dish only. It is a fair approximation, since most of the wind energy is absorbed by the tipping structure. The force distribution on the dish surface yields important information for

determining the wind action on the antenna. Based on the available quasi-static wind tunnel data (see Fox [7], Blaylock [8] and Levy and Kurtz [9]), the spatial force distribution is obtained from the JPL–IDEAS model by Levy and Strain [6]. As a result, the wind force as a time and spatial variable becomes a time variable in the dynamic model. The force acting on the dish has two components F_x and F_y (wind from x- and y-directions). The x-component is the wind force acting along the elevation axis, and the y-component is the horizontal force orthogonal to the elevation axis. Since the time characteristics of the wind force do not depend on its direction, the wind force is further denoted F.

The statistical properties of the wind force are determined from the already described wind velocity parameters. At a given height, the force is proportional to the square of the velocity (see Velozzi and Cohen [14]):

$$F = kv^2, \tag{7}$$

and the velocity consists of a constant mean flow with a superimposed fluctuation, as in equation (1). Thus, the force is decomposed into a steady force F_m and a turbulent force F_t with zero mean value

$$F = F_m + F_t. \tag{8}$$

The steady-state force F_m (lb) is determined for the speed v_m (mph) as

$$F_m = F(v_m) = kv_m^2 = \alpha_w^2 F_{0m}, \tag{9}$$

where $\alpha_w = v_m/100$, $F_{0m} = 1$ lbf is the force at wind velocity 100 mph, and $k = 0{\cdot}0001F_{0m}$. The gust F_t, on the other hand, is determined as

$$F_t = \alpha_f v_t, \tag{10}$$

where $\alpha_f = (\partial F/\partial v)|_{v=v_m} = 2kv_m = 2F_m/v_m$ depends on wind velocity v_m. From equation (10), the wind force spectrum is obtained as

$$S_f(f) = \alpha_f^2 S_v(f), \tag{11}$$

and thus the standard deviation σ_f of the gust is

$$\sigma_f = |\alpha_f|\sigma_v. \tag{12}$$

Finally, introducing equation (6) in equation (12), one obtains

$$\sigma_f = \alpha F_m \tag{13}$$

for the steady state force F_m given by equation (9).

3. WIND FORCE SIMULATIONS

Steady state and dynamic wind forces have been simulated. The steady state force is determined from equation (9). The dynamic force is generated by a filter with a transfer function $T(f)$,

$$T(f) = [a_0 + a_1 s + a_2 s^2 + \cdots + a_{m-1} s^{m-1}]/[b_0 + b_2 s + b_2 s^2 + \cdots + b_m s^m]. \tag{14}$$

The input of the filter is a random function of time (white noise). The parameters a_i, b_i, $i = 1, \ldots, m$, $m > 0$ are determined so that the power spectrum of $T(f)$ is the best approximation of the wind power spectrum $S_f(f)$. For this purpose, the square root s_f of the power spectrum S_f is used:

$$s_f(f) = \sqrt{S_f(f)}. \tag{15}$$

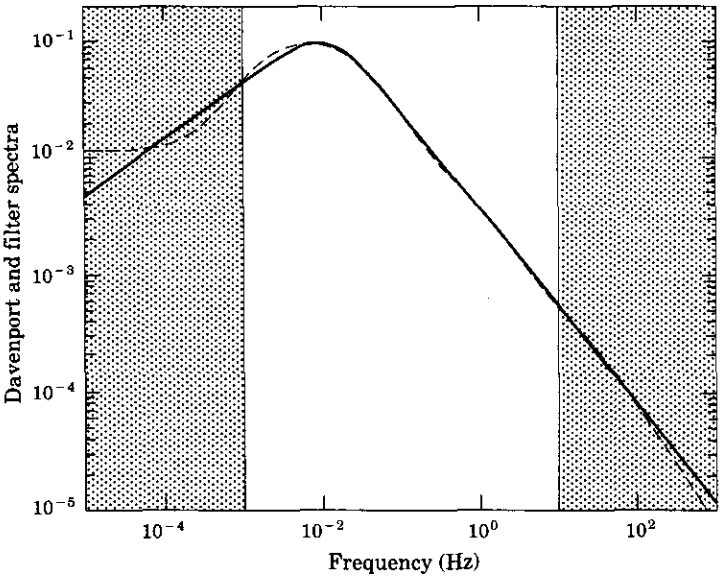

Figure 2. Plots of the square root of the power spectrum of the Davenport wind gust model, for a 30 mph wind at the DSS-13 antenna site (——); and the filter transfer function (– – –).

The order m of the filter, and the parameters $a_i, i = 1, \ldots, m-1$, $b_i, i = 1, \ldots, m$ are to be determined. For the frequency interval $[f_1, f_2]$, $f_2 > f_1$, denote the norm $\|\cdot\|_w$ of a function $g(f)$ as

$$\|g\|_w^2 = \int_{f_1}^{f_2} w(f) g^2(f)\, df, \tag{16}$$

where $w(f) > 0$ and $f \in [f_1, f_2]$ is a weighting function, and denote the poles of the transfer function $\lambda_i, i = 1, \ldots, m$; then the filter parameters and the filter order should be found so that the index J,

$$J = \|s_f(f) - |T(f)|\|_w, \tag{17}$$

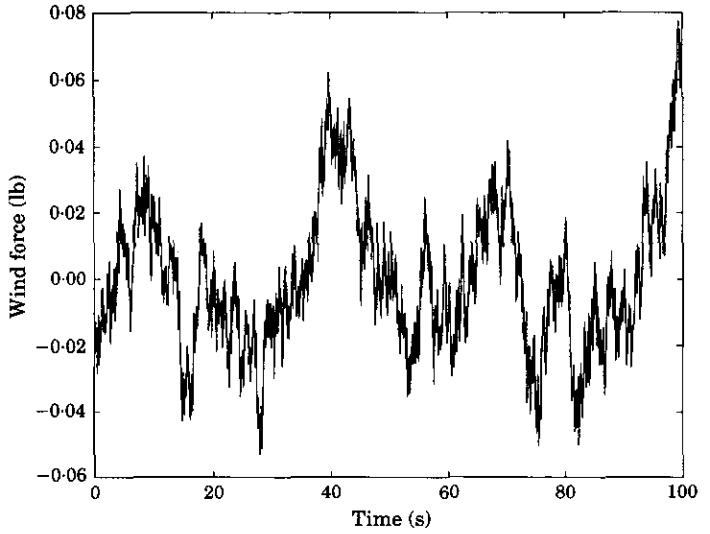

Figure 3. The wind force generated by the filter for the 30 mph wind gust.

is minimal, subject to the constraints

$$\mathrm{Re}\,(\lambda_i) < 0, \qquad \text{for } i = 1, \ldots, m. \tag{18}$$

The constraints assure filter stability.

The plot of the function $s_f(f)$, obtained from the Davenport model (15) for a wind speed of 30 mph, is shown in Figure 2 by the solid line. A linear filter which generates the wind force of a spectrum close to the Davenport model is determined by minimizing J subject to constraints (18). The values of the Davenport spectrum for high frequencies (in this case considered for frequencies 1–1000 Hz) are small, and therefore they should be weighted significantly in order to obtain a good fit in this frequency range. The following weights have been assigned: $w = 3$ for frequencies 0·1–1 Hz, $w = 10$ for 1–10 Hz, $w = 30$ for 10–100 Hz, and $w = 100$ for 100–1000 Hz. For different integers m, the index J has been minimized; the integer $m = 4$ was found to be the lowest filter order for which the results have been satisfactory. The filter parameters for the minimal solution are: $a_0 = -0{\cdot}6808$, $a_1 = 464{\cdot}7941$, $a_2 = -155{\cdot}8598$, $a_3 = -2{\cdot}6426$, $b_0 = -0{\cdot}3538$, $b_1 = -29{\cdot}5829$, $b_2 = -187{\cdot}2598$, $b_3 = -38{\cdot}2997$, $b_4 = -0{\cdot}3310$.

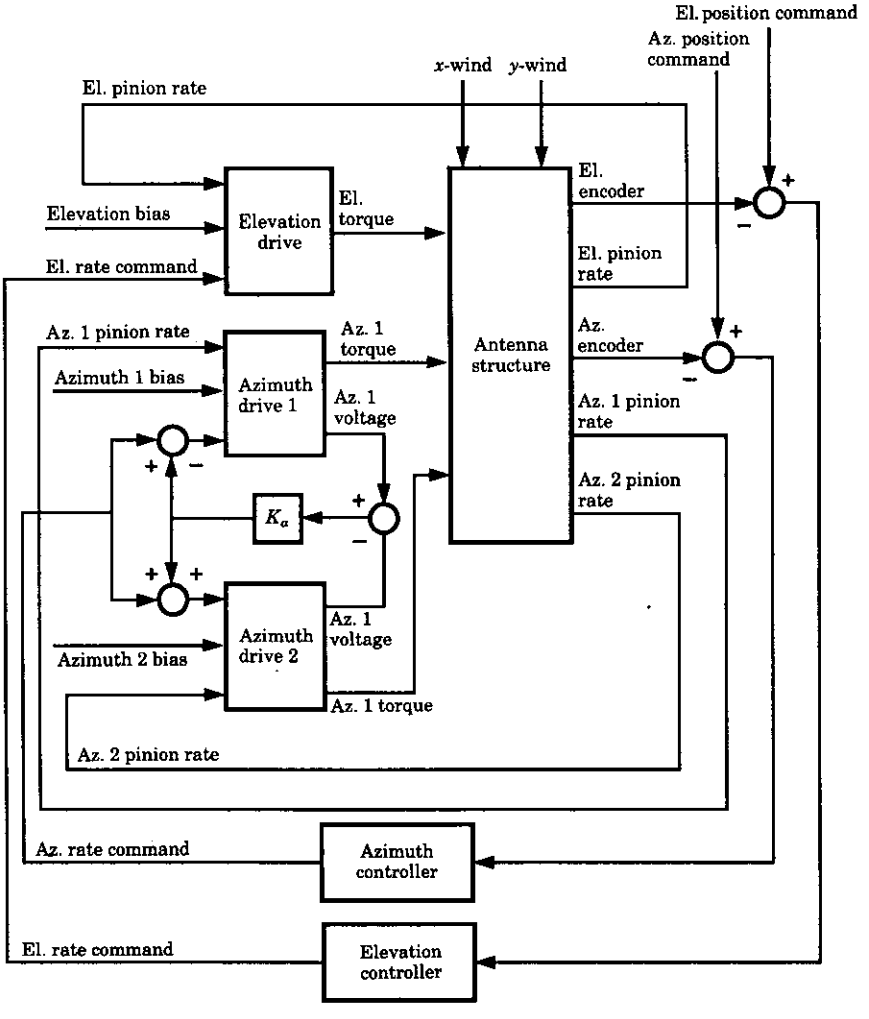

Figure 4. A block diagram of the antenna control system.

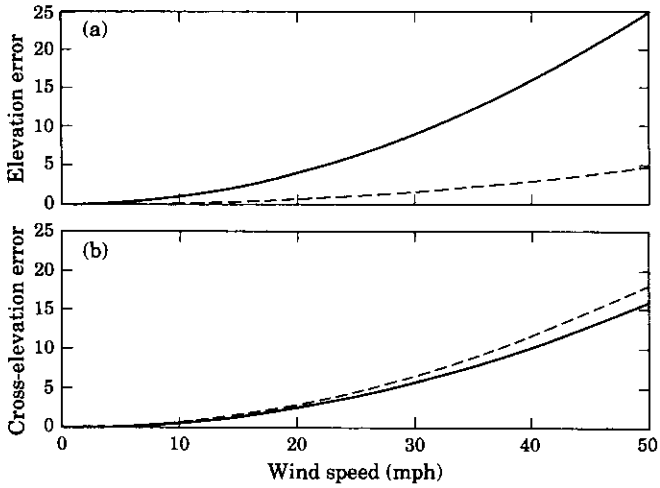

Figure 5. The pointing error due to a steady state wind from the x-direction: (a) elevation pointing error; (b) cross-elevation pointing error. ——, Antenna elevation position 60 degrees; – – – –, position 90 degrees.

The magnitude of the filter transfer function is shown in Figure 2 by the dashed line. The figure shows good approximation of the Davenport spectrum within the interval of interest $[f_1 = 0{\cdot}001, f_2 = 10]$ Hz. The wind force generated by the filter for a 30 mph wind is shown in Figure 3.

A similar approach was used to determine wind filters and wind forces for wind velocities $v_m = 10$, 20, 40 and 50 mph.

4. POINTING ERROR SIMULATIONS

The DSS-13 Deep Space Network antenna with a 34 m dish (see Figure 1) is analyzed in what follows. A block diagram of the antenna control system is shown in Figure 4. It consists of the antenna structure, elevation and azimuth drives, and elevation and azimuth controllers. A finite element structural model was developed, which has about 10 000

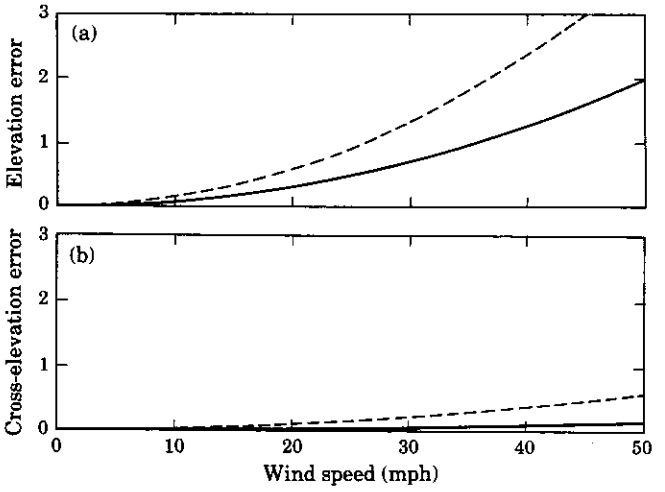

Figure 6. The pointing error due to a steady state wind from the y-direction: (a) elevation pointing error; (b) cross-elevation pointing error. ——, Antenna elevation position 60 degrees; – – – –, position 90 degrees.

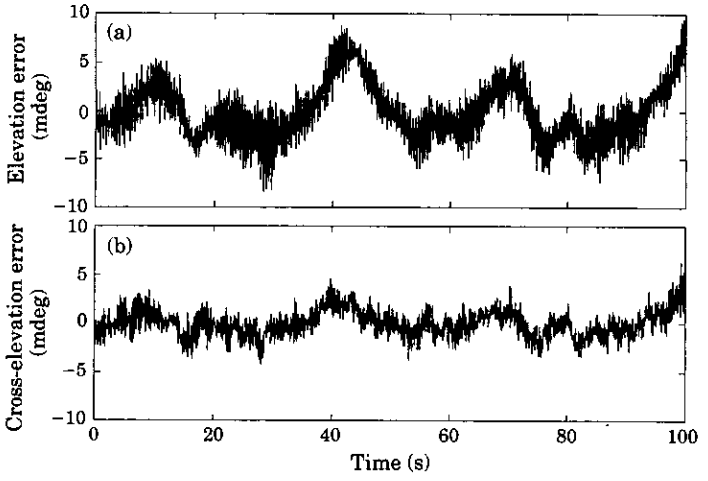

Figure 7. Antenna responses to x-direction wind gusts: (a) elevation pointing error; (b) cross-elevation pointing error.

degrees of freedom. For dynamics simulations the first 21 modes (with natural frequencies up to 10 Hz) were used. The state space model with position loop closed is described in detail by Gawronski and Mellstrom [4]. It consists of 90 states, reduced to 36 states using a balanced reduction technique [15–17] and is

$$\dot{x} = Ax + B_c u + B_w F, \qquad y = Cx + Du, \tag{19}$$

where x is a state vector, $n \times 1$, u is the command signal, $p \times 1$, F is the wind force, and y is the output, q $\times$ 1. The input matrix B_w is such that for a steady state wind of 161 km/h (100 mph), a steady state wind force of $F_{0m} = 4{\cdot}44$ N (1 lbf) is applied. In this paper, two elevation positions of the antenna are simulated: 90 degrees and 120 degrees (that is, 60 degrees with wind blowing from behind the dish).

Since the antenna model is linear, the steady state force and dynamic force are simulated separately, and superimposed if necessary. For the steady state wind disturbances, the system with the position loop closed is simulated with the zero command signal u (blind pointing), and constant wind disturbance F_m. The steady state response (elevation and

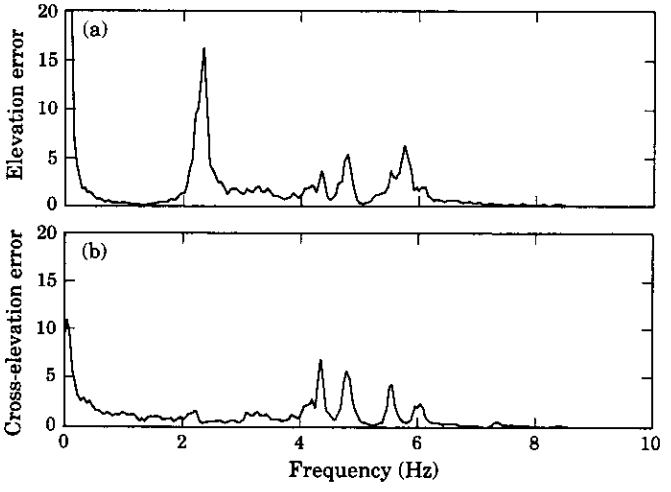

Figure 8. Spectra for x-direction wind gusts: (a) elevation pointing error; (b) cross-elevation pointing error.

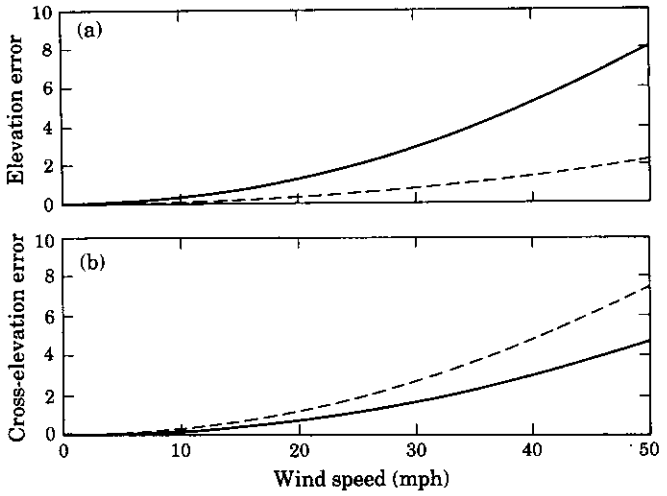

Figure 9. The quadratic law for x-direction wind gusts: (a) elevation pointing error; (b) cross-elevation pointing error. ——, Antenna elevation position 60 degrees; – – –, position 90 degrees.

cross-elevation pointing error) is obtained for 60 and 90 degree antenna elevation angles. Plots of the pointing error due to steady state wind from the x- and y-directions for different wind speeds are shown in Figures 5 and 6 (solid line for 60 degree elevation, dashed line for 90 degree elevation). The small pointing error due to wind in the y-direction is a result of the integrating action of the controller.

The gust wind load was applied to the antenna model. The responses of the antenna (EL and XEL pointing error) are presented in Figure 7 for an x-direction 30 mph wind, and the spectra of the x-wind 30 mph gust response are shown in Figure 8. They show that modes of low frequency (2 Hz), medium (4 Hz) and high frequency (6 Hz) are present in wind gust simulations; this information is given with respect to the controller bandwidth, and is vital in the design of antenna controllers with disturbance rejection properties.

Wind forces were simulated for velocities of 10, 20, 30, 40 and 50 mph for 60 and 90 degree elevation angles of the antenna. The results are presented in Figure 9 for an

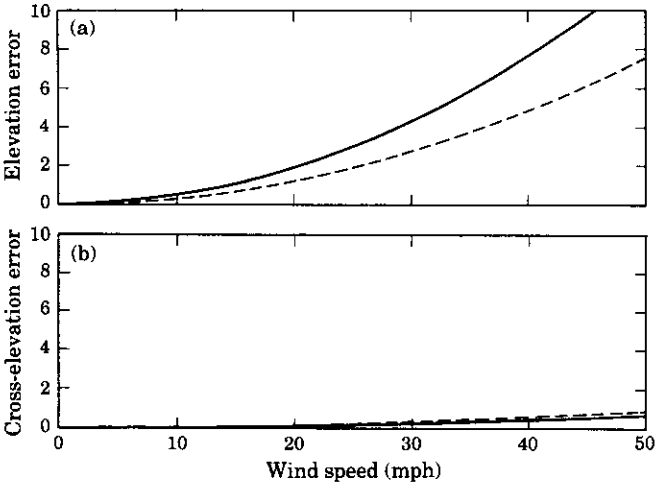

Figure 10. The quadratic law for y-direction wind gusts: (a) elevation pointing error; (b) cross-elevation pointing error. ——, Antenna elevation position 60 degrees; – – –, position 90 degrees.

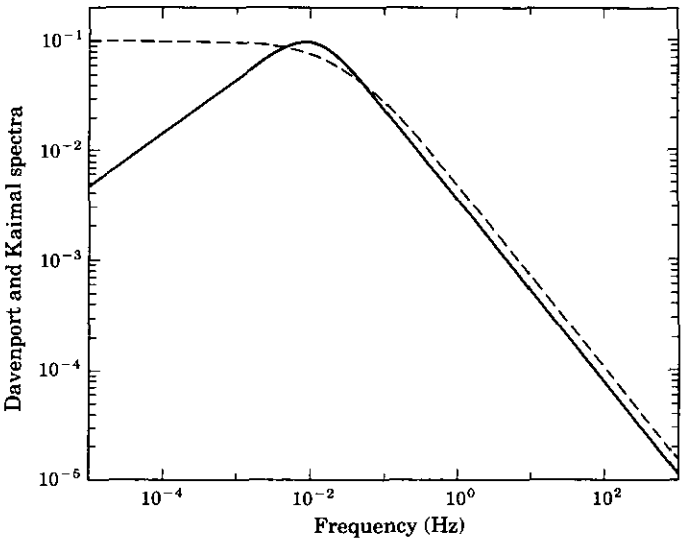

Figure 11. The square root of the 30 mph wind power spectrum at the DSS-13 antenna site of the Davenport model (——) and the Kaimal model (– – –).

TABLE 1

Comparison of the Davenport and Kaimal models

	Kaimal model		Davenport model	
	x-wind	y-wind	x-wind	y-wind
Elevation error (mdeg)	0·92	3·25	0·73	2·81
Cross-elevation error (mdeg)	2·87	0·40	2·37	0·32

x-direction wind and a 60 degree elevation angle (solid line), and a 90 degree elevation angle (dashed line), and in Figure 10 for a y-direction wind. Likewise, for the steady state load, the results of the dynamic loadings show the pointing errors to be proportional to the square of the velocity. It is seen from Figure 10 that the integrating action of the controller lowered a significant part of the pointing error due to steady state y-direction wind; however, the dynamic part of the y-direction wind is not compensated for by the controller, causing a significant pointing error.

For comparison, the Kaimal *et al.* wind model [18, 12] has been also simulated. The wind velocity spectrum

$$S_v(f) = 200\kappa v_m z/(1 + 50fz/v_m)^{5/3} \tag{20}$$

is compared with the Davenport spectrum in Figure 11. It is shown in the figure that the Kaimal spectrum overestimates the Davenport spectrum for almost all frequencies. The simulations of pointing error for a 30 mph wind for the antenna at zenith (90 degrees in elevation) are compared in Table 1. The table shows that the Kaimal model yields pointing error estimates that are 20% larger than the Davenport model.

5. CONCLUSIONS

Wind forces acting on the antenna structure have been modelled in this paper. Their steady state and dynamic parts have been applied as a disturbance to the closed loop

antenna model at 60 and 90 degrees of elevation angle. The results show that both the steady state and dynamic parts of the pointing error are of equal importance, and that despite the dominant presence of low frequency components in the wind disturbance spectrum, the high frequency modes of the antenna have been excited, causing significant pointing errors. The significant participation of wind gusts in the pointing error budget necessitates the design of antenna controllers with wind disturbance rejection properties.

ACKNOWLEDGMENTS

The authors would like to thank Darin Brekke, Roy Levy, Ben Parvin and Douglas Strain for their extensive discussions. This research was performed at the Jet Propulsion Laboratory, California Institute of Technology, under a contract with the National Aeronautics and Space Administration.

REFERENCES

1. M. S. KATOW and H. D. MCGINNESS 1973 *JPL Technical Report* 15. Wind load predictions for the 64-meter-diameter antenna.
2. M. S. KATOW 1975 *JPL Deep Space Network Progress Report* 42-49. Aerodynamic static differential pressure values for the 50 percent porous reflector dish.
3. M. MASSOUDI 1978 *TDA Progress Report* 42-43, 94–101. Tracking error of 100-m antenna due to wind gust.
4. W. GAWRONSKI and J. A. MELLSTROM 1994 in *Control and Dynamic Systems* (C. T. Leondes, editor) **67**. New York: Academic Press. Control and dynamics of the deep space network antennas.
5. G. BIERNSON 1990 *Optimal Radar Tracking Systems*. New York: John Wiley.
6. R. LEVY and D. STRAIN 1988 *JPL Internal Document* NPO-17783. JPL–IDEAS finite element analysis and design optimization program.
7. N. L. FOX 1962 *JPL Internal Memo* CP-4. Load distributions on the surface of paraboloidal reflector antennas.
8. R. B. BLAYLOCK 1964 *JPL Internal Memo* CP-6. Aerodynamic coefficients for model of a paraboloidal reflector directional antenna proposed for a JPL advanced antenna system.
9. R. LEVY and D. KURTZ 1978 *JPL Publication* 78-16. Compilation of wind tunnel coefficients for parabolic reflectors.
10. A. G. DAVENPORT 1961 *Journal of the Royal Meteorological Society* **87**, 194–211. The spectrum of horizontal gustiness near the ground in high winds.
11. R. LEVY and H. MCGINNESS 1976 *NASA Technical Memo* 33-802. Wind power prediction models.
12. E. SIMIU and R. H. SCANLAN 1986 *Wind Effects on Structures*. New York: John Wiley.
13. J. S. BENDAT and A. G. PIERSOL 1986 *Random Data*. New York: John Wiley.
14. J. VELLOZZI and E. COHEN 1968 *American Society of Civil Engineers, Journal of the Structural Division* **94**, 1295–1313. Gust response factors.
15. W. GAWRONSKI and T. WILLIAMS 1991 *Journal of Guidance, Control, and Dynamics* **14**, 68–76. Model reduction for flexible space structures.
16. W. GAWRONSKI and J.-N. JUANG 1990 in *Control and Dynamics Systems* (C. T. Leondes, editor) **36**, 143–222. New York: Academic Press. Model reduction for flexible structures.
17. W. GAWRONSKI and J. A. MELLSTROM 1992 *Journal of Guidance, Control and Dynamics* **15**, 1304–1306. Model reduction for systems and integrators.
18. J. C. KAIMAL, J. C. WYNGAARD, Y. IZUNI and O. R. COTE 1972 *Journal of the Royal Meteorological Society* **98**, 563–589. Spectral characteristics of surface-layer turbulence.